Soft X-ray Spectroscopy of C60/Copper Phthalocyanine/MoO3 Interfaces: Role of Reduced MoO3 on Energetic Band Alignment and Improved Performance

ARTICLE *in* THE JOURNAL OF PHYSICAL CHEMISTRY C · OCTOBER 2010

Impact Factor: 4.77 · DOI: 10.1021/jp1071428

5 AUTHORS, INCLUDING:

Sang Wan Cho
Yonsei University
65 PUBLICATIONS **777** CITATIONS
SEE PROFILE

Louis F. J. Piper
Binghamton University
99 PUBLICATIONS **1,842** CITATIONS
SEE PROFILE

Alexander Demasi
Boston University
33 PUBLICATIONS **766** CITATIONS
SEE PROFILE

Soft X-ray Spectroscopy of C_{60}/Copper Phthalocyanine/MoO_3 Interfaces: Role of Reduced MoO_3 on Energetic Band Alignment and Improved Performance

S. W. Cho, L. F. J. Piper, A. DeMasi, A. R. H. Preston, and K. E. Smith*

Department of Physics, Boston University, 590 Commonwealth Ave, Boston, Massachusetts 02215, United States

K. V. Chauhan, R. A. Hatton, and T. S. Jones

Department of Chemistry, University of Warwick, Coventry CV4 7AL, United Kingdom

Received: July 30, 2010; Revised Manuscript Received: September 17, 2010

The interfacial electronic structure of C_{60}/copper phthalocyanine (CuPc)/molybdenum trioxide (MoO_3) thin films grown in situ on indium tin oxide (ITO) substrates has been studied using synchrotron radiation-excited photoelectron spectroscopy in an attempt to understand the influence of oxide interlayers on the performance of small molecule organic photovoltaic devices. The MoO_3 layer on ITO is found to significantly increase the work function of the substrate and induces large interface dipoles and band bending at the CuPc/MoO_3 interface. The large band bending confirms the formation of an internal potential that assists hole extraction from the CuPc layer to the electrode. The electronic structure of the MoO_3 layer on ITO was also examined using various soft X-ray spectroscopies to probe the conductive nature of the MoO_3 thin film.

I. Introduction

Organic photovoltaic (OPV) devices are the subject of considerable attention due to their potential technological benefits including low cost, mechanical flexibility, and light weight.[1−3] However, despite significant recent advances in cell performance, current power conversion efficiencies remain too low to make such cells commercially viable. A general problem in organic electronic devices is the poor transport of charge carriers at the interface between the electrodes and the organic semiconductor. Consequently, recent efforts have been expended in order to improve the charge transport and collection at the electrodes. In particular, the use of transition metal oxides as an interlayer between the indium tin oxide (ITO) transparent conducting electrode and the organic material has attracted considerable interest.[4] ITO is widely used as the substrate in OPV device fabrication due to its reasonable transparency in the visible region of the spectrum, good conductivity, and easy patterning ability. However, the surface chemistry of ITO is difficult to control.[5] Insertion of transition metal oxide interlayers is believed to prevent unwanted chemical reactions between the ITO substrate and the optically active organic layer.[4] Furthermore, a high work function material such as a metal oxide is desirable to decrease the series resistance in the devices.[6] Organic light emitting diodes (OLEDs)[7,8] and organic thin film transistors (OTFTs)[9,10] that include a MoO_3 interlayer have shown good properties regardless of the metal or conducting oxide used as the electrode. A MoO_3 interlayer has also been used in OPV cells and significantly improved device performance has been demonstrated for some organic materials systems, including improved power conversion efficiency and stability.[6] For example, in small molecule OPV cells based on chloro-aluminum phthalocyanine (ClAlPc/C_{60}) planar heterojunctions, the power conversion efficiency was found to increase from 1.6 to 2.6% after insertion of a 5 nm MoO_3 interlayer at the ITO substrate.[11]

MoO_3/organic and ITO/MoO_3 interfaces have been studied by several groups in order to explain the origin of the improvement in hole injection in OLEDs and OTFTs.[12−15] However, the origin of the performance improvement in OPV devices and the conduction mechanism for MoO_3 thin films remain unclear. Moreover, the charge transport shown in previous reports could not be possible if the MoO_3 interlayer behaved as a perfect insulator.

We report here a study of the electronic structure of MoO_3 layers grown on ITO and of the electronic structure of small molecule organic overlayers (CuPc/C_{60} heterojunctions) grown on the oxide layers. The electronic structure was measured using synchrotron radiation-excited photoelectron spectroscopy (PES), X-ray absorption spectroscopy (XAS), and X-ray emission spectroscopy (XES). Our goals were first to study the electronic structure of MoO_3 layers deposited on clean ITO substrates in order to understand the conduction mechanism of the oxide interlayer and then to study the interfacial electronic structures and energy level alignments at C_{60}/CuPc/MoO_3 interfaces to clarify the origin of the reported improvement in OPV devices when using MoO_3 interlayers. We also compared the molecular orientation of CuPc molecules deposited on MoO_3 and ITO surfaces using angle-dependent XAS as this may have an impact on the electronic energy level alignment at the interface and resulting device performance.

II. Experimental Details

Experiments were carried out at the soft X-ray undulator beamline X1B at the National Synchrotron Light Source (NSLS), Brookhaven National Laboratory. Multilayer structures of MoO_3/ITO and C_{60}/CuPc/MoO_3/ITO were grown in a custom designed ultra high vacuum (UHV) organic molecular beam deposition (OMBD) chamber (base pressure 2×10^{-9} Torr), attached to a multitechnique soft X-ray spectroscopy system,

* To whom correspondence should be addressed. E-mail: ksmith@bu.edu.

10.1021/jp1071428
Published on Web 10/05/2010

described below. Clean ITO surfaces were obtained via Ar^+ ion sputtering and annealing in UHV. MoO_3 was deposited on the ITO substrate and then CuPc and C_{60} were deposited onto the MoO_3 substrate from well outgassed thermal evaporators in sequence. The substrate was at room temperature during deposition, and the film deposition rate was monitored by a quartz crystal microbalance. The deposition rate for MoO_3 was 10 Å/s, and the rate for the organics was 0.5 Å/s. After deposition, the samples were transferred under vacuum into the spectrometer chamber (base pressure 2×10^{-10} Torr).

Beamline X1B is equipped with a spherical grating monochromator, and the photon beam is focused to an approximate 60×40 μm spot on the sample. PES spectra were recorded using a Scienta 100 mm hemispherical electron analyzer. The O 1s and Mo 3d core level spectra were excited using an incident photon energy of 750 eV. The secondary electron cutoff and valence band PES spectra were recorded using an incident photon energy of 250 eV. The onset of photoemission (and hence the sample work function) was measured with a negative bias (−9 V) applied to the sample in order to exceed the work function of the detector. Spectra are referenced relative to the Fermi level (E_F) of an atomically clean gold foil in contact with the sample. O and N *K*-edge XAS spectra were recorded by the sample drain current technique to obtain the total electron yield (TEY) and were normalized to the current from a Au coated mesh positioned in the incident photon beam. The energy scale of the XAS measurements was calibrated using first- and second-order diffraction Ti *L*-edge and O *K*-edge absorption features of rutile TiO_2.[16] XES spectra were recorded with a Nordgren-type grazing incidence grating spectrometer.[17] The XES energies were calibrated to emission from the *L*-edge of a reference Zn film in the second-order of diffraction.[18]

Density functional theory (DFT) calculations were performed with the commercially available Gaussian 03 code.[19] The molecular geometry was optimized and molecular orbital energies, wave functions, and charge densities were obtained using a Becke-style 3-parameters hybrid functional (B3LYP). 6-31G* Gaussian basis sets, which have given reliable results for organic materials,[20,21] were used. We simulated the density of states by convolving each molecular level with the Gaussian functions having full-widths at half-maximum (fwhm) of 0.4 eV to compare with the experimental spectrum. The effect of the photoionization cross-section was also considered in the simulation.[22,23]

III. Results and Discussion

i. Electronic Structure of MoO_3 on ITO. Figure 1a shows how the work function (as measured from the secondary electron cutoff in PES) varies with the thickness of a MoO_3 film grown on ITO. The secondary electron cutoff shifts toward high work function with the deposition of MoO_3, with the shift saturating after deposition of a 5 nm film. The total shift is 2.45 eV, which corresponds to the work function change. This shows the formation of a large interface dipole on ITO due to the large work function of MoO_3. The magnitude of the interface dipole is in good agreement with previous reports.[12] Figure 1b presents valence band PES collected within 14 eV of E_F from ITO and the MoO_3 film grown on ITO. It shows the changes for the valence band from clean ITO to a 20 nm thick MoO_3 layer. The valence band of MoO_3 extending from 3−10 eV is mainly composed of O 2p states, with only a very minor contribution from Mo 4d states, while the conduction band is dominated by Mo 4d states with some hybridization with O 2p states.[24] However, the spectra in Figure 1 reveal a weak emission feature

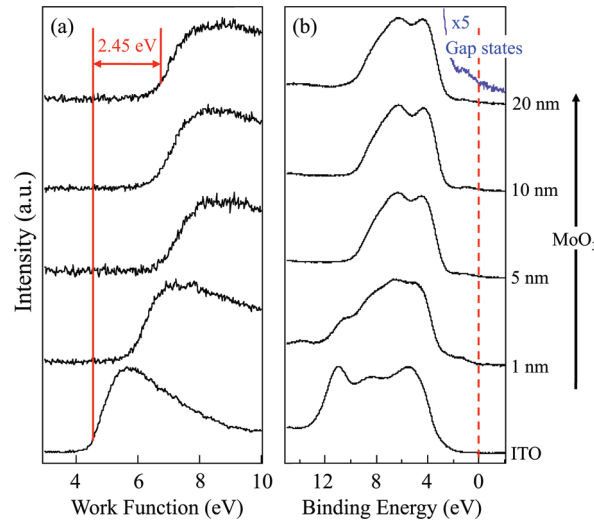

Figure 1. (a) Change in the onset of secondary electron PES spectra after the deposition of MoO_3 layer on ITO. (b) Valence band PES spectra recorded near E_F after the deposition of MoO_3 layer on ITO.

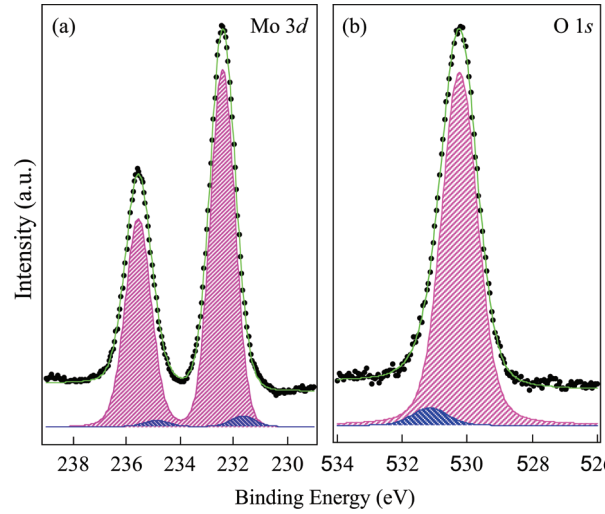

Figure 2. (a) Mo 3d and the O 1s core-level photoemission spectra from MoO_3 thin films. $h\nu_{excite} = 750$ eV.

close to E_F which is not expected on the basis of the insulating properties of MoO_3. This gap state is likely to be related to a hybridized occupied Mo 4d−O 2p state and is associated with O vacancy defects, since no such feature is observed for stochiometric MoO_3.[25] The existence of a reduced MoO_{3-x} phase is also supported by the Mo 3d core level spectra presented in Figure 2a.

Figure 2 displays Mo 3d and O 1s core level photoemission spectra from 20 nm thick MoO_3 films grown on ITO. The line shapes of these spectra were analyzed by a standard least-squares fitting scheme using a convolution of Gaussian and Lorentzian peaks. The width of the Lorentzian peaks was assumed to be the same for each component. We obtain a fwhm for the Lorentzian of about 0.20 eV for Mo 3d and 0.30 eV for O 1s. The fwhm for the Gaussian resulting from the fitting procedure is 1.10−1.25 eV and is similar for each component. The Mo 3d core level spectrum is dominated by a spin−orbit doublet with peaks at binding energies of 232.40 and 235.55 eV. Both the binding energy and spin−orbit splitting are in good agreement with values previously reported for MoO_3.[24,26] In addition, a low intensity doublet peak at lower binding energy was observed, as shown in Figure 2a. This indicates that there is a slight reduction in the MoO_3 layer. The O 1s binding energy

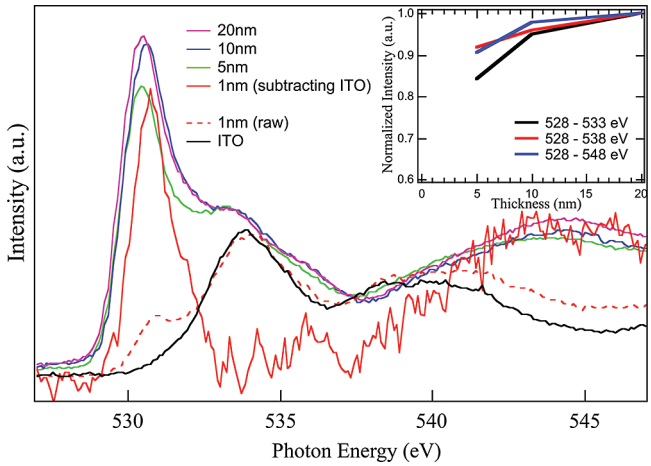

Figure 3. O *K*-edge XAS spectra as function of MoO_3 thickness on ITO. The inset shows the relation between the area intensity of each region and the film thickness (5, 10, and 20 nm).

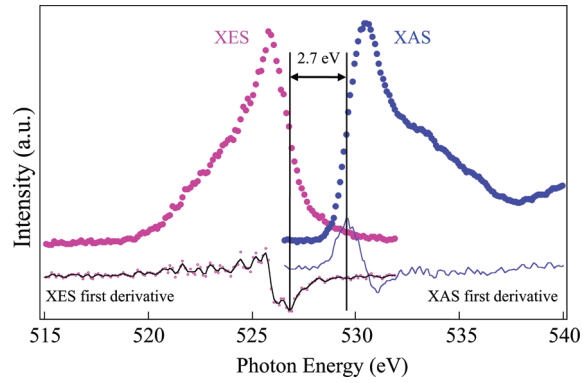

Figure 4. Soft XAS and nonresonant XES from 200 nm thick MoO_3 at the O *K*-edge. The band gap is determined from the XAS and nonresonant XES spectra by taking the derivative of the spectra to locate the inflection point in the valence band and conduction band onset.

for MoO_3 was measured to be 530.25 eV, also in good agreement with previous reported values.[24,26] The O vacancies do not affect the main O 1s binding energy,[26] but a small satellite peak was also observed at higher binding energy as shown in Figure 2b. Similar O 1s spectra for MoO_3 and MoO_2 have been previously reported.[24,27] Although the exact origin remains unclear, the most probable explanation is that this satellite arises from the existence of surface OH groups.[24]

As shown in Figure 1b, occupied gap states are observed in the MoO_{3-x} layer. The resultant MoO_{3-x} layer does not therefore behave as a perfect insulator, in contrast to what one would naturally expect for MoO_3. Closer inspection of the spectra in Figure 1 reveals that emission from the gap states is strongest from very thin films (1 nm thick MoO_3) compared to the thicker films. This suggests that the thinnest oxide layer has the greatest number of oxygen vacancies, and the gap state is associated with O vacancy defects as mentioned above. To confirm this, we recorded O *K*-edge XAS spectra as a function of film thickness, as shown in Figure 3. The intensity of the features in these spectra is proportional to the density of unoccupied states and the oxygen concentration. Consequently, the decrease in spectral weight observed in Figure 3 as a function of MoO_3 thickness is a direct reflection of a decrease in the number of O 2p holes and an increase in the number of electrons, both linked to the occurrence of oxygen vacancies.[28] However, in the spectrum from the 1 nm film, the features of MoO_3 and ITO overlap because 1 nm is smaller than the inelastic mean free path length (IMFP) for electrons at these energies. We have subtracted the ITO contribution from the XAS spectrum recorded from the 1 nm thick MoO_3 film, but the intensity is still very low and the second spectral feature is not fully formed. This means that the 1 nm thick film is clearly below the TEY saturation limit. Therefore, we have compared the intensity differences using the spectra from 5, 10, and 20 nm thick films. Above 5 nm the ITO contribution is negligible because TEY signals are dominated by contributions from the first 5 nm of a sample. The inset shows the relation between the area intensity of the main peak and film thickness because most of the changes should be in the pre-edge region if oxygen vacancies were related. There is a trend in the area shape with increasing intensity with thickness. As mentioned above, this implies that the thinner oxide layer has more oxygen vacancies and is more conductive. The higher defect density in the thinnest films is likely due the ease with which MoO_3 can be reduced at the initial deposition stage via interaction with background hydrogen or the substrate. However, as the MoO_3 layers get thicker, such effects diminish. Note however that while a reduction of MoO_3 has been observed following deposition of some organic molecules (for example *N*,*N*′-bis(1-naphthyl)-*N*,*N*′-diphenyl-1,1′-biphenyl-4,4′-diamine (NPB)), we see no evidence of a reduction following CuPc deposition.[12] However the work function for the thin films is smaller than that of the thicker layers. Therefore, we estimate that 5−10 nm is the optimum thickness of the MoO_3 interlayer for a compromise between good electrical conductivity and a sufficiently large work function for use in organic devices such as OPVs.

Figure 4 shows O *K*-edge XAS and nonresonant XES data for a thick (200 nm) MoO_3 layer. O *K*-edge (1s → 2p excitations) XAS is an accurate method to determine the unoccupied O 2p partial density of states (PDOS) in transition-metal oxides since the ligand core hole created by photoexcitation is highly screened from the band-edge electronic states localized on the metal sites.[29,30] Similarly, O *K*-edge XES spectra excited with photons with energy significantly above the O 1s absorption threshold (nonresonant excitation) reflect directly the occupied O 2p PDOS. Gilbert et al. have recently determined the band gap for iron oxide from O *K*-edge XAS and nonresonant XES spectra by taking the derivative to locate the inflection points in the valence band and conduction band onset.[31] They propose this method as an internally consistent approach for determining the band gap from XAS and XES spectra for other transition metal oxides. By use of this method, we estimate the band gap for the MoO_3 film to be 2.7 eV, which is a little smaller than the reported value (2.98−3.37 eV).[13,32] In general, the final state in XAS includes a core-hole, which prevents absolute comparison between the energy scales of XAS and XES.[33] Therefore, to obtain the exact band gap, the core-hole binding energy (0.5−1.0 eV) should be considered.[34,35] However, McLeod et al. have reported that the effect of the core hole on XAS spectra becomes progressively weaker as the cation becomes more massive.[36] It has been also reported the decrease in energy band gap of MoO_3 with increasing substrate temperature is due to oxygen vacancies.[37] Consequently, the estimated band gap for our MoO_3 films is reasonable.

ii. Electronic Structure of C_{60}/CuPc/MoO_3. Figure 5a shows how the work function (as measured from the cutoff energy in PES) varies with the thickness of a CuPc film and with subsequent deposition of a C_{60} film on the CuPc layer. The cutoff position shifted toward lower work function immediately after the 1 nm CuPc layer was deposited. The abrupt shift of the secondary cutoff in the earliest stages of film growth is attributed to formation of an interface dipole.[38] In general, if

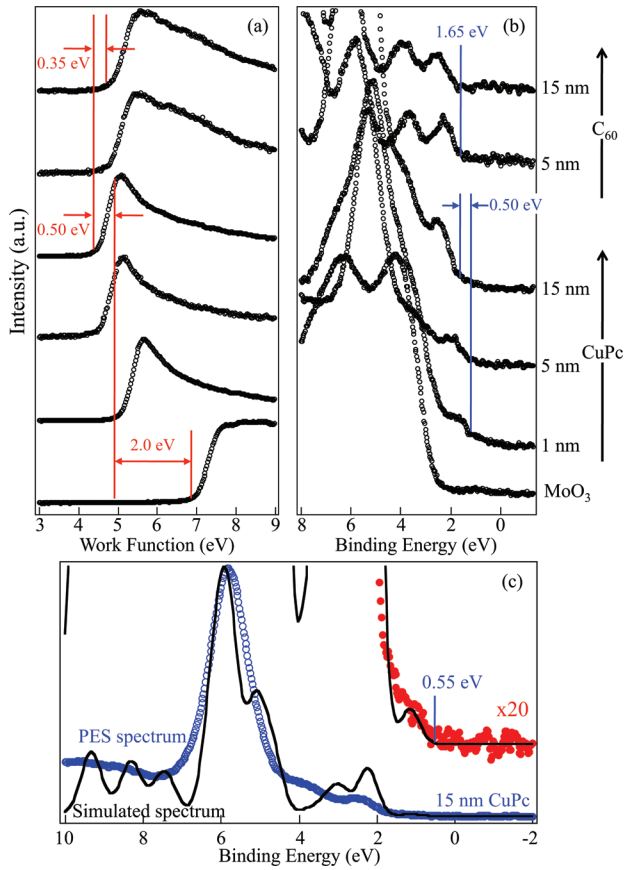

Figure 5. (a) Change in the onset of secondary electron PES spectra after the deposition of each layer of C_{60}/CuPc/MoO_3. (b) Valence band PES spectra recorded near E_F after the deposition of each layer of C_{60}/CuPc/MoO_3. (c) Comparison between valence band PES and the simulated spectrum for CuPc from DFT calculation.

the work function of an electrode exceeds the ionization potential of an organic material, the misalignment between the two Fermi levels leads to electron transfer from the organic material to the electrode layer until thermodynamic equilibrium is established, thus generating a dipole to reduce the work function.[39,40] Recent results of the electronic structures of MoO_3 clearly explain the electron transfer from a-NPD the highest occupied molecular orbital (HOMO) to the MoO_3 layer.[13,14] Most important result is that the MoO_3 has an extremely large electron affinity (6.7 eV). Similarly, our results show the electron affinity of MoO_3 (6.9 eV) exceeds the ionization potential of CuPc (5.0 eV) and the Fermi level of MoO_3 is pinned near its conduction band edge due to the occupied gap states. Therefore, the electron can be directly transferred from the HOMO of CuPc to the conduction band of MoO_3, and this charge transfer gives a large interface dipole. As more CuPc was deposited, the cutoff position moved a little more toward lower work function and the total shift of the cutoff position of CuPc was 2.5 eV. The magnitude of the dipole was estimated to be 2.0 eV at the CuPc/MoO_3 interface after subtracting the contribution of downward band bending (see below). Subsequent deposition of C_{60} resulted in a shift of the interface dipole between C_{60} and CuPc of 0.35 eV to higher energy. Figure 5b presents valence band photoemission spectra collected within 8 eV of E_F from MoO_3, from the CuPc films grown on MoO_3, and then from the C_{60}/CuPc/MoO_3 multilayer. As thicker CuPc films are deposited, it is clear that the CuPc occupied molecular orbitals shift toward higher binding energies and the total energy shift reaches 0.5 eV at saturation. This confirms that downward band bending occurs at the CuPc/MoO_3 interfaces as implied by the data in Figure 5a. Note that the photoemission intensity from HOMO state of CuPc is very weak because the photoionization cross sections for C 2p and N 2p are much smaller than that for Cu 3d at these incident photon energies. To define the exact HOMO onset, we compared it with the simulated spectrum for CuPc from DFT calculations (Figure 5c). The simulated spectrum is in reasonable agreement with the experimental PES spectrum. The exact HOMO onset can be defined and the saturation HOMO onset of the CuPc layer was 0.55 eV below E_F. By contrast, there was no shift in the HOMO energy for the C_{60}/CuPc interface. The HOMO onset of the C_{60} layer deposited on the CuPc layer was measured as 1.65 eV. We can also estimate the lowest unoccupied molecular orbital (LUMO) onset of the C_{60} layer (0.35 eV) from the previously reported band gap of 2.0 eV.[41] The energy difference between the HOMO onset of the donor (CuPc) and the LUMO onset of the acceptor (C_{60}) ($E^{D}_{HOMO} - E^{A}_{LUMO}$) is a strong factor in determining the magnitude of the measured open-circuit voltage (V_{OC}) of an OPV cell based on a donor−acceptor heterojunction.[42,43]

Figure 6 presents the energy level diagram for C_{60}/CuPc/ITO and C_{60}/CuPc/MoO_3/ITO. The ionization potentials of CuPc and C_{60} are estimated to be about 4.95 eV and 6.30−6.40 eV, in agreement with previous reports.[44−47] The measured $E^{D}_{HOMO} - E^{A}_{LUMO}$ differences were 0.9 and 1.0 eV with and without the MoO_3 interlayer, respectively. However, the difference in the V_{OC} values measured in OPV devices fabricated on ITO and MoO_3/ITO is negligible (0.04−0.05 eV) according to previous results.[6] Thus the $E^{D}_{HOMO} - E^{A}_{LUMO}$ difference of 0.1 eV is not enough to modify the V_{OC} in OPVs, most likely because other factors such as the energy to dissociate the bound electron−hole pair at the donor/acceptor interface should be considered.[48] Cattin et al. have suggested that the main improvement induced by a MoO_3 interlayer between ITO and CuPc is related to the fill factor (FF),[6] with higher FFs attributed to a reduction in carrier recombination.[49] To understand the origin of this effect, we examined the band alignments at the CuPc/MoO_3 interface in greater detail. As noted above, the measured interface dipole and band bending are 2.0 and 0.5 eV, respectively. Since the MoO_3 layer significantly increases the work function of the substrate, it induces large interface dipoles and band bending at the CuPc/MoO_3 interface. From an energy perspective, when a negative voltage is applied to an electrode to attract holes, the potential difference bends the HOMO levels toward E_F. In other words, this large band bending results in the formation of an internal potential due to the work function difference between MoO_3 and CuPc. Moreover, it leads to a positive accumulation at the contact, no barrier, and an Ohmic contact. The internal potential enhances hole extraction from the CuPc layer to the substrate as if a negative voltage is applied on the substrate. Therefore, it reduces the carrier recombination that decreases the FF in OPVs. The existence of the internal potential between metal oxides and organic semiconductors has been previously reported for organic thin film transistors.[50]

An additional factor that has a major impact on the performance of OPV devices is the short exciton diffusion length of organic semiconductors, which is much less than the optical absorption length.[51] Carrier mobility has been found to improve if the organic molecules are well ordered in the thin film, since the order may increase the exciton diffusion length and enhance the carrier transport efficiency.[49,52] Therefore, we studied the molecular orientation of CuPc on ITO and MoO_3 using angle-dependent XAS. Figure 7a presents N *K*-edge XAS spectra from CuPc on ITO. Spectra recorded with the *p*-polarized radiation

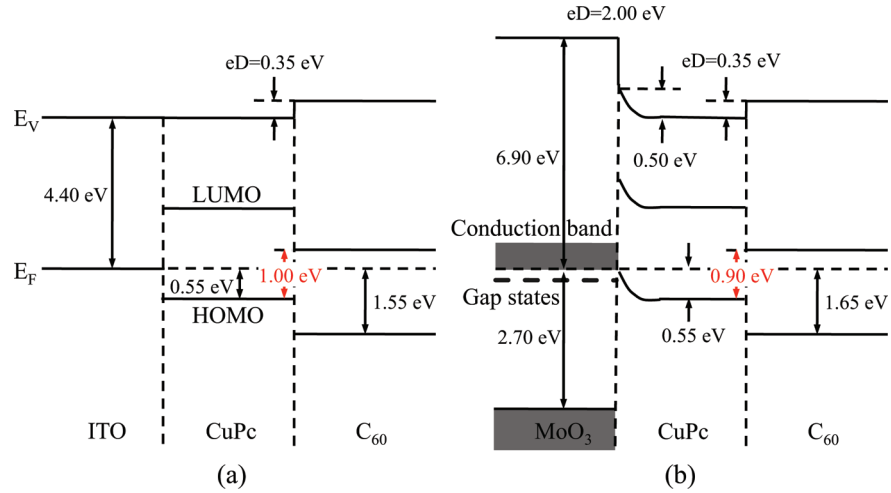

Figure 6. Energy level alignment of (a) C_{60}/CuPc/ITO and (b) C_{60}/CuPc/MoO_3/ITO.

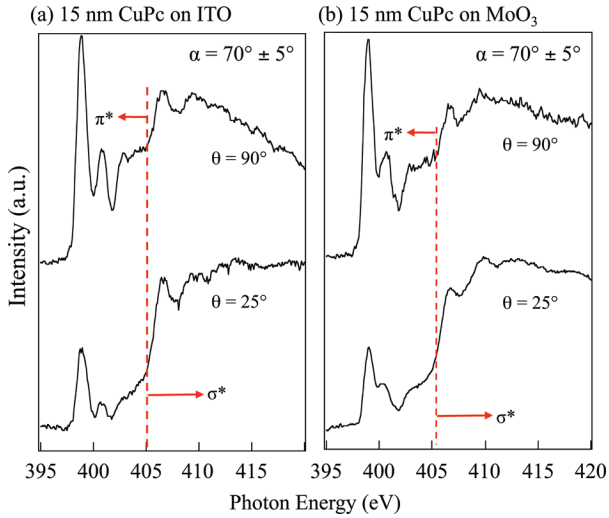

Figure 7. (a) N *K*-edge XAS spectra for CuPc on ITO and (b) CuPc on MoO_3.

incident at $\theta = 25$ and 90° to the sample surface are shown. It can be seen that the relative intensity of the π^* and σ^* resonances change significantly with incident angle. The CuPc molecules are relatively well ordered on the ITO surface, as reported previously.[53] The intensity (I) of the π^* resonance in the XAS spectra (photon energy range 397−405 eV) is related to the tilt angle, α, of the CuPc molecular plane with respect to the substrate plane and the photon incidence angle, θ, by[54]

$$I(\theta) \propto 1 + \frac{1}{2}(3\cos^2\theta - 1)(3\cos^2\alpha - 1)$$

By use of this formula, we estimate the azimuthal average tilt angle α to be 70 ± 5° for CuPc on ITO. Figure 7b presents N *K*-edge XAS spectra from CuPc on MoO_3. The spectra show almost the same relative intensity of the π^* and σ^* resonances as a function of incident angle of the X-ray beam. Thus the CuPc molecules deposited on MoO_3 are also reasonably well ordered, and the molecular orientation of CuPc on both surfaces is similar. We conclude therefore that the MoO_3 interlayer does not alter the molecular orientation of the CuPc donor molecules.

IV. Conclusions

The interfacial electronic structure of C_{60}/CuPc/MoO_3 grown on ITO has been investigated using in situ synchrotron radiation-excited photoelectron spectroscopy to understand the effect of including ultrathin oxide interlayers at the hole extracting electrode in small molecule OPVs. Because the MoO_3 layer significantly increases the work function of the substrate, it induces a large interface dipole and band bending at the CuPc/MoO_3 interface. The large band bending confirms the formation of an internal potential that will enhance hole extraction from the CuPc layer to the substrate. The metallic nature of the MoO_3 layer was also shown to be due to O vacancy defects.

Acknowledgment. This work was supported in part by the NSF under Grant No. CHE-0807368. The NSLS is supported by the U.S. Department of Energy, Office of Science, Office of Basic Energy Sciences, under Contract No. DE-AC02-98CH10886. Financial support from the EPSRC, UK is also acknowledged through the SUPERGEN Excitonic Solar Cell Consortium programme. R.A.H. is grateful to the Royal Academy of Engineering/EPSRC for the award of a Fellowship.

References and Notes

(1) Peumans, P.; Yakimov, A.; Forrest, S. R. *J. Appl. Phys.* **2003**, *93*, 3693.
(2) Brabec, C. J.; Sariciftci, N. S.; Hummelen, J. C. *Adv. Funct. Mater.* **2001**, *11*, 15.
(3) Xue, J. G.; Uchida, S.; Rand, B. P.; Forrest, S. R. *Appl. Phys. Lett.* **2004**, *84*, 3013.
(4) Shrotriya, V.; Li, G.; Yao, Y.; Chu, C. W.; Yang, Y. *Appl. Phys. Lett.* **2006**, *88*, 073508.
(5) Kim, J. S.; Friend, R. H.; Grizzi, I.; Burroughes, J. H. *Appl. Phys. Lett.* **2005**, *87*, 023506.
(6) Cattin, L.; Dahou, F.; Lare, Y.; Morsli, M.; Tricot, R.; Houari, S.; Mokrani, A.; Jondo, K.; Khelil, A.; Napo, K.; Bernede, J. C. *J. Appl. Phys.* **2009**, *105*, 034507.
(7) You, H.; Dai, Y. F.; Zhang, Z. Q.; Ma, D. G. *J. Appl. Phys.* **2007**, *101*, 026105.
(8) Matsushima, T.; Kinoshita, Y.; Murata, H. *Appl. Phys. Lett.* **2007**, *91*, 253504.
(9) Kumaki, D.; Umeda, T.; Tokito, S. *Appl. Phys. Lett.* **2008**, *92*, 013301.
(10) Chu, C. W.; Li, S. H.; Chen, C. W.; Shrotriya, V.; Yang, Y. *Appl. Phys. Lett.* **2005**, *87*, 193508.
(11) Hancox, I.; Chauhan, K. V.; Sullivan, P.; Hatton, R. A.; Moshar, A.; Mulcahy, C. P. A.; Jones, T. S. *Energy Environ. Sci.* **2010**, *3*, 107.
(12) Lee, H.; Cho, S. W.; Han, K.; Jeon, P. E.; Whang, C. N.; Jeong, K.; Cho, K.; Yi, Y. *Appl. Phys. Lett.* **2008**, *93*, 043308.
(13) Kroger, M.; Hamwi, S.; Meyer, J.; Riedl, T.; Kowalsky, W.; Kahn, A. *Org. Electron.* **2009**, *10*, 932.
(14) Kroger, M.; Hamwi, S.; Meyer, J.; Riedl, T.; Kowalsky, W.; Kahn, A. *Appl. Phys. Lett.* **2009**, *95*, 123301.
(15) Jeon, P.; Han, K.; Lee, H.; Kim, H. S.; Jeong, K.; Cho, K.; Cho, S. W.; Yi, Y. *Synth. Met.* **2009**, *159*, 2502.

(16) Chen, X.; Glans, P. A.; Qiu, X.; Dayal, S.; Jennings, W. D.; Smith, K. E.; Burda, C.; Guo, J. *J. Electron Spectrosc. Relat. Phenom.* **2008**, *162*, 67.

(17) Nordgren, J.; Bray, G.; Cramm, S.; Nyholm, R.; Rubensson, J. E.; Wassdahl, N. *Rev. Sci. Instrum.* **1989**, *60*, 1690.

(18) *X-ray Data Booklet*; 2nd ed.; Thompson, A. C., Vaughan, D., Attwood, D. T., Gullikson, E. M., Howells, M. R., Kortright, J. B., Robinson, A. L., Underwood, J. H., Kim, K. J., Kirz, J., Lindau, I., Pianetta, P., Winick, H., Williams, G. P., Scofield, J. H., Eds.; Lawrence Berkeley National Laboratory, University of California, Berkeley, CA: Berkeley, California USA, 2001.

(19) Frisch, M. J.; Trucks, G. W.; Schlegel, H. B.; Scuseria, G. E.; Robb, M. A.; Cheeseman, J. R.; Montgomery, J. A., Jr.; Vreven, T.; Kudin, K. N.; Burant, J. C.; Millam, J. M.; Iyengar, S. S.; Tomasi, J.; Barone, V.; Mennucci, B.; Cossi, M.; Scalmani, G.; Rega, N.; Petersson, G. A.; Nakatsuji, H.; Hada, M.; Ehara, M.; Toyota, K.; Fukuda, R.; Hasegawa, J.; Ishida, M.; Nakajima, T.; Honda, Y.; Kitao, O.; Nakai, H.; Klene, M.; Li, X.; Knox, J. E.; Hratchian, H. P.; Cross, J. B.; Bakken, V.; Adamo, C.; Jaramillo, J.; Gomperts, R.; Stratmann, R. E.; Yazyev, O.; Austin, A. J.; Cammi, R.; Pomelli, C.; Ochterski, J. W.; Ayala, P. Y.; Morokuma, K.; Voth, G. A.; Salvador, P.; Dannenberg, J. J.; Zakrzewski, V. G.; Dapprich, S.; Daniels, A. D.; Strain, M. C.; Farkas, O.; Malick, D. K.; Rabuck, A. D.; Raghavachari, K.; Foresman, J. B.; Ortiz, J. V.; Cui, Q.; Baboul, A. G.; Clifford, S.; Cioslowski, J.; Stefanov, B. B.; Liu, G.; Liashenko, A.; Piskorz, P.; Komaromi, I.; Martin, R. L.; Fox, D. J.; Keith, T.; Al-Laham, M. A.; Peng, C. Y.; Nanayakkara, A.; Challacombe, M.; Gill, P. M. W.; Johnson, B.; Chen, W.; Wong, M. W.; Gonzalez, C.; Pople, J. A. *Gaussian 03*, revision C.02; Gaussian, Inc.: Wallingford, CT, 2004.

(20) Zhang, R. Q.; Lu, W. C.; Lee, C. S.; Hung, L. S.; Lee, S. T. *J. Chem. Phys.* **2002**, *116*, 8827.

(21) Cho, S. W.; Yi, Y.; Seo, J. H.; Kim, C. Y.; Noh, M.; Yoo, K. H.; Jeong, K.; Whang, C. N. *Synth. Met.* **2007**, *157*, 160.

(22) Yeh, J. J. *Atomic Calculation of Photoionization Cross-Sections and Asymmetry Parameters*; Gordon and Breach Science Publishers: Langhorne, PA, 1993.

(23) Yeh, J. J.; Lindau, I. *Atomic Data Nucl. Data Tab.* **1985**, *32*, 1.

(24) Scanlon, D. O.; Watson, G. W.; Payne, D. J.; Atkinson, G. R.; Egdell, R. G.; Law, D. S. L. *J. Phys. Chem. C* **2010**, *114*, 4636.

(25) Tokarz-Sobieraj, R.; Hermann, K.; Witko, M.; Blume, A.; Mestl, G.; Schlogl, R. *Surf. Sci.* **2001**, *489*, 107.

(26) Fleisch, T. H.; Mains, G. J. *J. Chem. Phys.* **1982**, *76*, 780.

(27) Belatel, H.; Al-Kandari, H.; Al-Khorafi, F.; Katrib, A.; Garin, F. *Appl. Catal., A* **2004**, *275*, 141.

(28) Herng, T. S.; Qi, D.-C.; Berlijn, T.; Yi, J. B.; Yang, K. S.; Dai, Y.; Feng, Y. P.; Santoso, I.; Sanchez-Hanke, C.; Gao, X. Y.; Wee, A. T. S.; Ku, W.; Ding, J.; Rusydi, A. *Phys. Rev. Lett.* 2010. in press.

(29) de Groot, F. M. F.; Grioni, M.; Fuggle, J. C.; Ghijsen, J.; Sawatzky, G. A.; Petersen, H. *Phys. Rev. B* **1989**, *40*, 5715.

(30) Mackrodt, W. C.; Jollet, F.; Gautier-Soyer, M. *Philos. Mag. B* **1999**, *79*, 25.

(31) Gilbert, B.; Frandsen, C.; Maxey, E. R.; Sherman, D. M. *Phys. Rev. B* **2009**, *79*, 035108.

(32) Julien, C.; Khelfa, A.; Hussain, O. M.; Nazri, G. A. *J. Cryst. Growth* **1995**, *156*, 235.

(33) Vonbarth, U.; Grossmann, G. *Phys. Rev. B* **1982**, *25*, 5150.

(34) Tezuka, Y.; Shin, S.; Agui, A.; Fujisawa, M.; Ishii, T.; Yagishita, A. *J. Electron Spectrosc. Relat. Phenom.* **1996**, *79*, 195.

(35) Preston, A. R. H.; Ruck, B. J.; Piper, L. F. J.; DeMasi, A.; Smith, K. E.; Schleife, A.; Fuchs, F.; Bechstedt, F.; Chai, J.; Durbin, S. M. *Phys. Rev. B* **2008**, *78*, 155114.

(36) McLeod, J. A.; Wilks, R. G.; Skorikov, N. A.; Finkelstein, L. D.; Abu-Samak, M.; Kurmaev, E. Z.; Moewes, A. *Phys. Rev. B* **2010**, *81*, 245123.

(37) Sivakumar, R.; Gopalakrishnan, R.; Jayachandran, M.; Sanjeeviraja, C. *Curr. Appl. Phys.* **2007**, *7*, 51.

(38) Ishii, H.; Sugiyama, K.; Ito, E.; Seki, K. *Adv. Mater.* **1999**, *11*, 605.

(39) Fukagawa, H.; Kera, S.; Kataoka, T.; Hosoumi, S.; Watanabe, Y.; Kudo, K.; Ueno, N. *Adv. Mater.* **2007**, *19*, 665.

(40) Braun, S.; Salaneck, W. R.; Fahlman, M. *Adv. Mater.* **2009**, *21*, 1450.

(41) Brumbach, M.; Placencia, D.; Armstrong, N. R. *J. Phys. Chem. C* **2008**, *112*, 3142.

(42) Chauhan, V.; Hatton, R.; Sullivan, P.; Jones, T.; Cho, S. W.; Piper, L.; deMasi, A.; Smith, K. *J. Mater. Chem.* **2010**, *20*, 1173.

(43) Cho, S. W.; Piper, L. F. J.; DeMasi, A.; Preston, A. R. H.; Smith, K. E.; Chauhan, K. V.; Sullivan, P.; Hatton, R. A.; Jones, T. S. *J. Phys. Chem. C* **2010**, *114*, 1928.

(44) Kera, S.; Yabuuchi, Y.; Yamane, H.; Setoyama, H.; Okudaira, K. K.; Kahn, A.; Ueno, N. *Phys. Rev. B* **2004**, *70*, 085304.

(45) Wu, C. I.; Hirose, Y.; Sirringhaus, H.; Kahn, A. *Chem. Phys. Lett.* **1997**, *272*, 43.

(46) Zahn, D. R. T.; Gavrila, G. N.; Gorgoi, M. *Chem. Phys.* **2006**, *325*, 99.

(47) Hayashi, N.; Ishii, H.; Ouchi, Y.; Seki, K. *J. Appl. Phys.* **2002**, *92*, 3784.

(48) Rand, B. P.; Burk, D. P.; Forrest, S. R. *Phys. Rev. B* **2007**, *75*, 115327.

(49) Yu, B.; Huang, L.; Wang, H.; Yan, D. *Adv. Mater.* **2010**, *22*, 1017.

(50) Cho, S. W.; Jeong, J. G.; Park, S. H.; Cho, M. H.; Jeong, K.; Whang, C. N.; Yi, Y. *Appl. Phys. Lett.* **2008**, *92*, 213302.

(51) Forrest, S. R. *Mater. Res. Soc. Bull.* **2005**, *30*, 28.

(52) Li, L. Q.; Tang, Q. X.; Li, H. X.; Hu, W. P. *J. Phys. Chem. B* **2008**, *112*, 10405.

(53) Peisert, H.; Schwieger, T.; Auerhammer, J. M.; Knupfer, M.; Golden, M. S.; Fink, J.; Bressler, P. R.; Mast, M. *J. Appl. Phys.* **2001**, *90*, 466.

(54) Stöhr, J. *NEXAFS Spectroscopy*; Springer: Berlin, 1992.

JP1071428